S.T. Yau High School Science Award

Research Report

The Team

Team member: Shengtian Hong

School: Milton Academy

City, Country: Milton, Massachusetts 02186, USA

Instructor: Xuan Luo

Job Title: Principal Scientist

Institution: National Graphene Research and Development Center

City, Country: Springfield, Virginia 22151, USA

Title of Research Report: 2-Thiouracil Antithyroid Drug Delivery with Functionalized BC_3 Monolayers: A First-principles Study

Date: August 21st, 2025

2-Thiouracil Antithyroid Drug Delivery with Functionalized BC_3 Monolayers: A First-principles Study

Shengtian Hong

Abstract

2-Thiouracil ($C_4H_4N_2OS$), an antithyroid drug (ATD) used in the treatment of Graves' disease and thyroid storm, requires an effective drug delivery vehicle to reach the thyroid gland successfully. Using first-principles calculations, the adsorption of the 2-Thiouracil molecule on pristine, Si-doped, and Al-doped BC_3 monolayers was studied based on the Density Functional Theory (DFT). Our results show that chemisorption of 2-Thiouracil is stronger on Si-doped than Al-doped BC_3, while pristine BC_3 shows weak physisorption. On the doped monolayers, the O atom on 2-Thiouracil displayed bond formation, hybridization, and stronger adsorption to the dopants than the S atom. We concluded that out of the 10 configurations computed, 2T-O_h/Si-BC_3 had the largest adsorption energy, making it the most promising configuration for future antithyroid drug delivery research. Our findings highlight how doped BC_3 monolayers can act as effective drug delivery platforms for the antithyroid drug, potentially improving the treatment of Graves' disease with future experimental validation.

Keywords: Density functional theory, First-principle calculations, 2D materials, BC_3, 2-Thiouracil, Graves' disease, Drug delivery.

Acknowledgement

Shengtian Hong completed the research and writing process under the guidance of Dr. Luo. Moreover, we would like to thank Dr. Gefei Qian for providing technological support. There was no financial assistance received for this study.

Commitments on Academic Honesty and Integrity

We hereby declare that we

1. are fully committed to the principle of honesty, integrity and fair play throughout the competition.
2. actually perform the research work ourselves and thus truly understand the content of the work.
3. observe the common standard of academic integrity adopted by most journals and degree theses.
4. have declared all the assistance and contribution we have received from any personnel, agency, institution, etc. for the research work.
5. undertake to avoid getting in touch with assessment panel members in a way that may lead to direct or indirect conflict of interest.
6. undertake to avoid any interaction with assessment panel members that would undermine the neutrality of the panel member and fairness of the assessment process.
7. observe the safety regulations of the laboratory(ies) where we conduct the experiment(s), if applicable.
8. observe all rules and regulations of the competition.
9. agree that the decision of YHSA is final in all matters related to the competition.

We understand and agree that failure to honour the above commitments may lead to disqualification from the competition and/or removal of reward, if applicable; that any unethical deeds, if found, will be disclosed to the school principal of team member(s) and relevant parties if deemed necessary; and that the decision of YHSA is final and no appeal will be accepted.

(Signatures of full team below)

X 

Name of team member: Shengtian Hong

X _____

Name of team member:

X _____

Name of team member:

X 

Name of supervising teacher: **Xuan Luo**

Contents

I. INTRODUCTION

Graves' disease, an autoimmune disease characterized by an enlarged and overactive thyroid gland, affects millions of people globally.[1] Although Graves' disease itself is not life-threatening, it can lead to thyroid storm,[2] which has a death rate of 25%,[3] and potentially raise the incidence rate of thyroid cancer by 10.4 times in an individual.[4] Therefore, research institutes and pharmaceutical industries have done extensive research related to the treatment of Graves' disease, including conducting thyroidectomy surgery and the use of radioactive iodine.[5] Although effective, these methods are costly and invasive, involving either surgical removal or destruction of the thyroid tissue. Moreover, they carry a post-therapy hypothyroidism rate exceeding 80 %.[6] Due to these drawbacks, patients often choose to receive a more cost-effective and nonablative treatment method, the use of antithyroid drugs(ATDs),[6,7] such as 2-Thiouracil ($C_4H_4N_2OS$), which require drug delivery vehicles to deliver them into the thyroid tissue.[8]

Scientists have done extensive research on drug delivery vehicles, including zero-dimensional nanoparticles, one-dimensional nanotubes and nanocones, etc.[9,10] In 2014, Paolino's team aimed to conjugate one-dimensional nanoliposomes to the thyroid-stimulating hormone(TSH), and found the system to be effective in the treatment of many thyroid diseases.[11] Zhang's team evaluated, in 2020, the combination of anti-thyroid cancer drug 5-fluorouracil with a porous Ba(NO3)2 organic framework, and proved the structure's efficacy against cancer cells.[12] In 2023, Harismah's group studied the potential combination of 2-Thiouracil with Be-doped Carbon Nanocone, finding that the models were desirable for the use of drug delivery against hypothyroidism.[13] In recent years, 2D monolayers have also been broadly studied as a carrier for drugs due to their large surface areas and relatively small quantum sizes, enhancing their efficacy in comparison to other nanocarriers.[14,15] For example, Pari and his team analyzed, in 2021, the combination of an iron-assisted carbon monolayer for the delivery of 2-Thiouracil, and discovered the dominant role of the monolayer for managing interactions with the drug.[16] Within 2D monolayers, graphene is used prominently in the field of drug delivery due to its chemical stability and large surface area, allowing efficient drug loading.[17,18] For instance, Dastani's team concluded, in 2020, that graphene and functionalized graphene nanosheets can be used as carriers for the Cladribine

anticancer drug molecule.[19] Moreover, metal-doped graphene, as Khodadadi et al. discovered in 2019, has a stronger adsorption behavior to the anticancer drug beta-lapachone compared to that of pristine graphene, and doped graphene nanosheets can have a better effect in the delivery of the drug.[20] Similarly, graphene-like monolayers, such as BCN,[21] MgO,[22] BaO,[22] BeS,[23] and BC_3,[24] all exhibit similar exceptional properties, and their implications in drug delivery have been studied.

With its exceptional chemical properties,[25] the BC_3 monolayer was studied by Rahimi et al. and combined with the nirosourea anticancer drug in 2020, and the results showcase a large adsorption energy, demonstrating the potential application of BC_3 in drug delivery.[26] In 2021, Chen et al. calculated that BC_3 had a larger adsorption energy when combined with the anticancer drug 5-fluorouracil than that of graphene-like NC3 and that of pristine graphene, confirming that the Boron Carbide monolayer could be used as a potential carrier for drug delivery application.[27] Furthermore, previous studies have shown the effectively increased adsorption energy, signifying stronger interactions, when molecules such as formaldehyde[28] and acetone,[29] were combined with Si-doped and Al-doped BC_3 compared to pristine BC_3. Therefore, we assert that the graphene-like BC_3 monolayer showcases high strength and conductivity, while the potential isovalent, substitutional doping with Si and Al could benefit the adsorption of the drug, making pristine, Si-doped, and Al-doped BC_3 optimal monolayers for this study.

Currently, the 2-Thiouracil molecule's adsorption on pristine, Si-doped, and Al-doped BC_3 has not been studied. While this study is theoretical, understanding adsorption behavior is a crucial step in evaluating whether functionalized BC_3 monolayers could act as a viable drug delivery nanocarrier under biological conditions. Other key factors, such as biocompatibility, stability, and targeted delivery to the thyroid tissue, will ultimately determine the clinical efficacy of this system, but adsorption energy trends can determine promising configurations for *in vitro* research.

The first-principle calculations based on the density functional theory (DFT)[30] are used in this study to evaluate the effectiveness of pristine, Si-doped, and Al-doped BC_3 monolayer as drug carriers for 2-Thiouracil. Calculations were conducted to find the optimal structure of each monolayer, as well as to determine adsorption energy, band structure, total and projected density of states (DOS), and charge transfer on 2-Thiouracil on pristine and doped

BC_3 monolayers. The calculated results of 2-Thiouracil's adsorption on each monolayer were then compared and analyzed to find the optimal monolayer for the delivery of 2-Thiouracil. In the second section, we explain our computation methods; in the third section, we display our results and discussions on 2-Thiouracil adsorption; finally, the fourth section showcases our conclusions.

II. METHOD

A. Computational Details

First-principles calculations were performed based on the Density Functional Theory (DFT) within the Generalized Gradient Approximation (GGA) in Perdew-Burke-Ernzerhof (PBE) format implemented in the ABINIT code.[31] The Projected Augmented Wave (PAW) method[32] was used to generate the pseudopotentials of elements with the ATOM PAW.[33] Elements in this study include hydrogen, boron, carbon, nitrogen, oxygen, aluminum, silicon, and sulfur. Table I shows all corresponding electron configurations and radius cutoffs of all elements studied.

TABLE I: Electron configuration and radius cutoff r_{cut} (Bohr) of elements studied for generating PAW pseudopotential

Elements	Electron configuration	r_{cut} (Bohr)
Hydrogen(H)	$1s^1$	0.995
Boron(B)	$[He]2s^22p^1$	1.701
Carbon(C)	$[He]2s^22p^2$	1.507
Nitrogen(N)	$[He]2s^22p^3$	1.200
Oxygen(O)	$[He]2s^22p^4$	1.415
Aluminum(Al)	$[Ne]3s^23p^1$	1.904
Silicon(Si)	$[Ne]3s^23p^2$	1.909
Sulfur(S)	$[Ne]3s^23p^4$	1.915

For total energy calculations, the self-consistent field (SCF) iteration was considered converged when the total energy difference was smaller than 1.0×10^{-10} hartree twice con-

secutively. For accurate results, the kinetic energy cutoff, Monkhorst-Pack k-point grid, and vacuum heights were considered converged after the total energy difference of data sets was less than 0.0001 hartree (about 3 meV) twice consecutively. The relaxation of atomic structures was considered converged when the maximum absolute force on each atom was less than 2.0×10^{-4} hartree/Bohr (about 0.01 eV/Å).

B. Atomic Structures

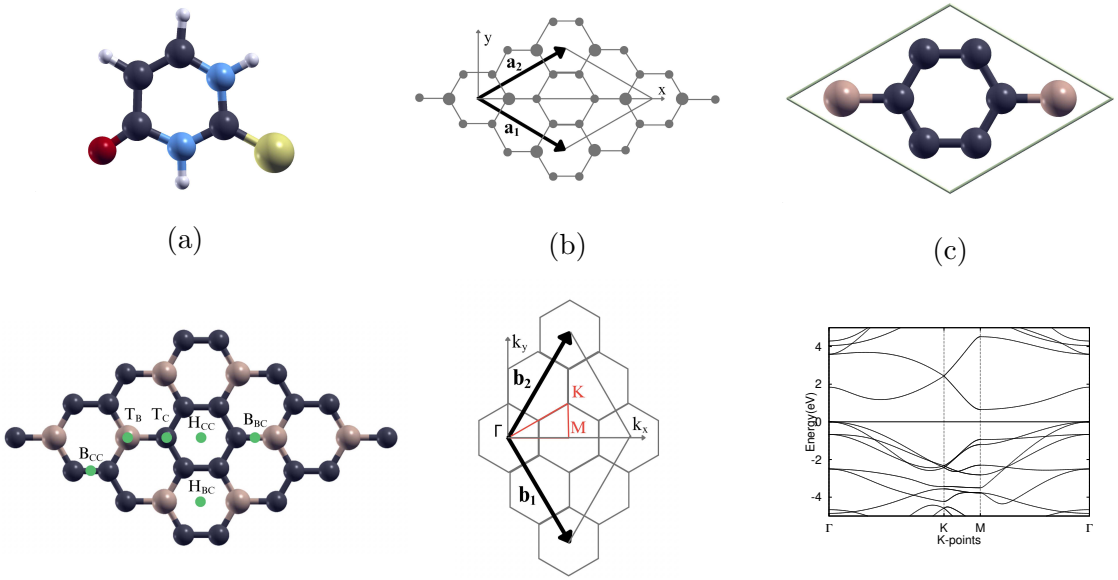

(a) (b) (c) (d) (e) (f)

FIG. 1: (a) The atomic structure of the 2-Thiouracil($C_4H_4N_2OS$) molecule, (b) the Bravais lattice ($\mathbf{a}_1$, $\mathbf{a}_2$) of the BC_3 monolayer, (c) the atomic structure of the BC_3 primitive cell, (d) possible adsorption sites on the 2×2-BC_3 monolayer, (e) the reciprocal lattice ($\mathbf{b}_1$, $\mathbf{b}_2$) of the BC_3 monolayer, with the high symmetry k points in the first Brillouin zone Γ (0, 0, 0), K (1/3, 2/3, 0), and M (1/2, 1/2, 0), (f) the band structure of the BC_3 monolayer, with the Fermi level set to 0 eV and the high symmetry k point circuit in the following order Γ → K → M → Γ. For all atomic structures, hydrogen, nitrogen, oxygen, sulfur, carbon, and boron atoms are white, blue, red, yellow, purple, and beige, respectively.

1. 2-Thiouracil molecule The atomic structure of the 2-Thiouracil molecule ($C_4H_4N_2OS$), an effective antithyroid drug, is shown in Fig. 1(a). This planar, aromatic

pyrimidine ring has a carbonyl O, a thione group, and two N atoms in the ring.

2. Pristine BC_3 monolayer The BC_3 monolayer has a 2D hexagonal bravais lattice as shown in Fig. 1(b). The 8-atom primitive cell consisted of 2 B atoms and 6 C atoms is displayed in Fig. 1(c). The BC_3 monolayer was then scaled up to a 2×2 supercell with 32 atoms, as shown in Fig. 1(d). Fig. 1(e) displays the reciprocal lattice of the BC_3 monolayer, and the high symmetry k points in the first Brillouin zone are Γ (0, 0, 0), K (1/3, 2/3, 0), and M (1/2, 1/2, 0). The band structure of BC_3, shown in Fig. 1(f), was computed along the k point circuit $\Gamma \rightarrow K \rightarrow M \rightarrow \Gamma$. The direct band gap is between the VBM and CBM at Γ point.

3. Doped BC_3 monolayers To potentially improve 2-Thiouracil adsorption, the BC_3 monolayer was isovalently doped by substituting a carbon with a silicon (Si), and a boron with an aluminum (Al), in separate instances, creating the Si-doped-2×2-BC_3 (Si-BC_3) and Al-doped-2×2-BC_3 (Al-BC_3) monolayers.

The defect formation energy (E_f) is defined as

$$E_f = E_{doped-ML} - E_{pure-ML} - E_{dopant} + E_{sub} \tag{1}$$

where $E_{doped-ML}$, $E_{pure-ML}$, E_{dopant}, and E_{sub} are the chemical potentials of the doped monolayer, the pure monolayer, the dopant (Si or Al), and the substituted atom (C or B), respectively. Crystalline Si, crystalline Al, graphene, and orthorhombic B were used to compute chemical potentials for Si, Al, C, and B, respectively.

4. 2-Thiouracil-BC_3 complexes To place the 2-Thiouracil molecule on pristine BC_3 monolayer, adsorption sites were identified. On 2-Thiouracil, the O atom of the carbonyl and the S atom of the thione are considered reactive sites.

All possible adsorption sites for 2-Thiouracil on 2×2-BC_3 are shown in Fig. 1(d). T_B is directly on top of a B atom; T_C is directly on top of a C atom; B_{BC} means on the B-C bond; B_{CC} represents on the C-C bond; H_{BC} stands for in the B-C ring; and H_{CC} stands for in the ring with only C atoms.

Both reactive sites on 2-Thiouracil were placed onto each adsorption site on 2×2-BC_3 as possible configurations.

In doped monolayers, the dopant (Si or Al) was considered the main reactive site on the monolayer. Therefore, the O atom and S atom on 2-Thiouracil were both placed on

the Si dopant vertically and horizontally, resulting in four different positions on Si-BC_3. 2-Thiouracil was placed onto Al-BC_3 in a similar manner, except the vertical placement when S was on top of Al resulted in an unstable configuration, so only three positions are present.

The vacuum layers of 2-Thiouracil and BC_3 monolayers were calculated independently, and values were added as the vacuum layer of the drug-monolayer complex, while ensuring an additional buffer space.

Total energy calculations were then run for the monolayer-molecule complex, the isolated 2-Thiouracil molecule, and the isolated monolayers. Adsorption energy (E_{ad}) was defined by

$$E_{ad} = E_{mol+ML} - E_{ML} - E_{mol} \tag{2}$$

where E_{mol+ML}, E_{ML}, and E_{mol} represent the total energies of the complex, the monolayer, and the 2-Thiouracil molecule, respectively. A more negative adsorption energy demonstrates a more stable configuration as well as a stronger adsorption. Previous studies have stated that an adsorption energy smaller than -80 kJ/mol (around -0.83 eV/molecule) indicates chemisorption. Therefore, we classify adsorption energies smaller than -0.83 eV as chemisorption and energies larger than -0.83 eV as physisorption.[34]

C. Electronic Structures

1. Band structure The band structure for all optimized monolayers and molecule-monolayer complexes was calculated along high symmetry k-points Γ (0,0,0), K (1/3, 2/3, 0), and M (1/2, 1/2, 0) as shown in Fig. 1(b).

2. Density of states (DOS) Total DOS was calculated and compared with the band structure to further analyze distributions of the density of states at different energy levels, especially around the band gap. To further analyze the contributions of 2-Thiouracil adsorption on BC_3 monolayers to the density of states, projected DOS calculations were conducted using the tetrahedron method. The atoms chosen for projection are interacting atoms on the monolayer and the 2-Thiouracil molecule.

3. Charge transfer The complexes that demonstrated strong adsorption were selected for charge transfer calculations. Charge transfer in the molecule-monolayer complex

was determined by finding the difference in charge density between the combined materials and the separate constituents, as indicated in Eq. 3.

$$\Delta\rho(r) = \rho_{mol+ML}(r) - \rho_{ML}(r) - \rho_{mol}(r) \tag{3}$$

where $\Delta\rho$ represents the charge difference. ρ_{mol+ML}, ρ_{ML}, and ρ_{mol} represent the charge density of the molecule-monolayer complex, the monolayer, and the 2-Thiouracil molecule, respectively. We plot the isosurface to visually display charge density differences.

III. RESULTS AND DISCUSSION

The optimized atomic structures, adsorption energies, band structures, density of states, and charge transfer were calculated for the 2-Thiouracil molecule adsorbed on pristine, Si-doped, and Al-doped BC_3 monolayers using first-principles calculations.

A. Molecule and Monolayer Calculations

The calculated lattice constant for the primitive BC_3 cell, selected bond angles for the 2-Thiouracil molecule, and selected bond lengths for both the 2-Thiouracil molecule and the BC_3 monolayer are shown in Table II.

As shown in Table II, for the 2-Thiouracil molecule, the CO and CS bond lengths were calculated to be 1.22 and 1.65 Å, while previous calculations by Rani et al. showed similar results of 1.22 and 1.67;Å[35] Tiekink et al. have measured values of 1.23 and 1.68 Å[36] in experiment, making the error 0.81% and 1.78%, respectively. Our calculated results of the OCN and SCN bond angles are 119.8° and 122.4°, which are similar to previously calculated values of 120.0° and 122.3°;[35] Tiekink et al. showed experimental results of 119.2° and 122.2,[36] and the error values of 0.5% and 0.16% also confirm our calculations. Therefore, data from previous work demonstrates the reliability of our molecule calculations.

The primitive cell BC_3 calculations show a lattice constant of 5.17 Å, a BC bond length of 1.57 Å, and a CC bond length of 1.42 Å, which is consistent with previously calculated values of 5.17, 1.56, and 1.42, by Bafekry et al.;[37] Yanagisawa et al. measured these values to be 5.37, 1.56, and 1.42[38] in experiment, which result in reasonable error values of 3.72%, 0.64%, and 0%, respectively, confirming our monolayer calculations.

TABLE II: Current calculated, other theoretically calculated, and experimental structural parameters of 2-Thiouracil($C_4H_4N_2OS$) molecule and BC_3 monolayer. Error represents the relative difference between the current calculated and experimental data. Bond length d (Å), bond angle ∠ (°), and lattice constant a (Å) were compared.

	Parameter	Calculated	Other	Experimental	Error(%)
2-Thiouracil	d_{CO} (Å)	1.22	1.22[35]	1.23[36]	0.81
	d_{CS} (Å)	1.65	1.67[35]	1.68[36]	1.78
	$\angle_{OCN}$ (°)	119.8	120.0[35]	119.2[36]	0.50
	$\angle_{SCN}$ (°)	122.4	122.3[35]	122.2[36]	0.16
BC_3	a (Å)	5.17	5.17[37]	5.37[38]	3.72
	d_{BC} (Å)	1.57	1.56[37]	1.56[38]	0.64
	d_{CC} (Å)	1.42	1.42[37]	1.42[38]	0

Overall, the current calculated parameters for the 2-Thiouracil molecule and the BC_3 monolayer demonstrate excellent agreement with previous theoretical computations as well as experimental data, verifying our computational methods.

The optimized atomic and band structures of pristine, Si-doped, and Al-doped BC_3 can be found in Fig. 2(a), Fig. 2(b), Fig. 2(c), respectively. All three monolayers have visible direct band gaps between the VBM and CBM at Γ point.

The lattice constant, band gap, and defect formation energy of optimized monolayers are shown in Table III. BC_3 has the smallest lattice constant of 10.352 Å, while Si-BC_3 and Al-BC_3 has larger lattice constants of 10.526 and 10.535 Å, respectively; this difference is most likely due to the larger atomic radius of Si and Al compared to a C or B atom. In contrast to the 0.648 eV band gap of pristine BC_3, both Si-BC_3 (0.124 eV) and Al-BC_3 (0.166 eV) have smaller band gaps. Moreover, Si-BC_3 has a defect formation energy of 3.311 eV, which is smaller than that of Al-BC_3 (9.964 eV), indicating that it requires less energy to replace a C atom by a Si atom than to replace a B with an Al on the BC_3 monolayer.

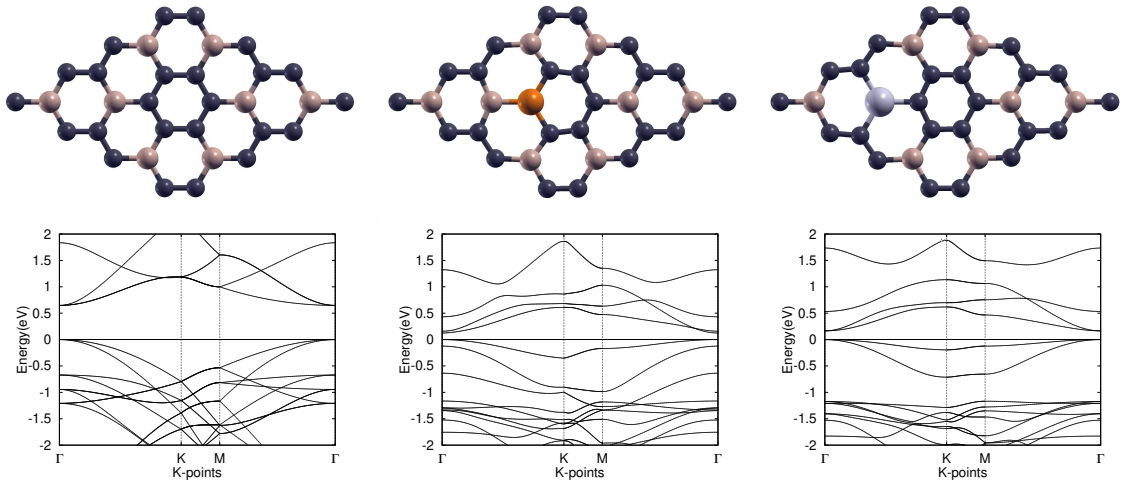

(a) (b) (c)

FIG. 2: (a) 2×2-BC_3, (b) Si-doped BC_3, (c) Al-doped BC_3. The first row shows the optimized atomic structures of the 3 monolayers, with carbon, boron, silicon, and aluminum atoms represented as purple, beige, blue, and grey, respectively. The second row displays the band structures of the 3 monolayers, with the Fermi level set to 0 eV; the high symmetry k point circuit runs in the following order $\Gamma \rightarrow K \rightarrow M \rightarrow \Gamma$.

TABLE III: Lattice constant a (Å), band gap E_g (eV), and defect formation energy E_f (eV) of pristine and doped BC_3 monolayers. Dir represents direct band gap.

Monolayer	a (Å)	E_g (eV)	E_f (eV)
BC_3	10.352	0.648 (dir)	N/A
Si-BC_3	10.526	0.124 (dir)	3.311
Al-BC_3	10.535	0.166 (dir)	9.964

B. 2-Thiouracil adsorbed on pristine BC_3

To place the 2-Thiouracil molecule on pristine BC_3, there are 9 potential adsorption sites, as shown in Fig. 1(d). In 2021, Z. Zhao et al. calculated the relaxation and adsorption of CH_3COCH_3 on BC_3, and they discovered an energy favorable position at the T_B site (top of a B atom) in pristine BC_3.[39] In a separate study by L. Zhao et al. in 2021, first-principles calculations indicated three stable adsorption sites, the hollow site of the carbon ring (H_{CC}),

the hollow site of the carbon-boron ring (H_{BC}), and on top of a B atom (T_B).[40] Therefore, the T_B, H_{BC}, and H_{CC} positions on pristine BC_3 were selected to initially place and potentially bind with reactive sites of 2-Thiouracil.

Although 2-Thiouracil was placed on T_B, H_{CC}, and H_{BC} sites initially, the O atom demonstrated affinity to the T_B site, and the S atom demonstrated affinity to the H_{BC} site after relaxation. In the relaxed configuration where 2-Thiouracil was horizontal, when O was on T_B, S was consequently pushed to a separate T_B site. The top and side views of the three optimized structures, 2T-O/BC_3, 2T-S/BC_3, and 2T-h/BC_3, are displayed in the top two rows of Fig. 3. In the 2T-O/BC_3 configuration, the molecule is vertical, with the O atom on the T_B site; 2T-S/BC_3 also represents a vertical position, with the S atom on the H_{BC} site; in 2T-h/BC_3, the molecule is horizontal, and both O and S atoms are on T_B sites. The computed band structures, total density of states (DOS), and projected DOS can be found below each atomic structure in Fig. 3. Adsorption energy, lattice constant, band gap, and binding distance of each complex are shown in Table IV.

1. 2T-O/BC_3

The optimized atomic structure of 2T-O/BC_3 is shown in Fig. 3(a). The binding distance, the distance between two closest atoms on the molecule and the monolayer, is 3.05 Å, as shown in Table IV.

As shown in the band structure, there is a direct band gap between the VBM and CBM at Γ point. After 2-Thiouracil adsorption, the band gap of BC_3 decreased from 0.648 eV to 0.619 eV, as shown in Table III and Table IV. This demonstrates 2-Thiouracil influence on the electronic structure. In the total DOS, the same band gap of 0.619 eV is displayed.

As shown in the projected DOS in Fig. 3(a), the electron states around and above the Fermi level, 0 eV, were contributed by mostly the B_{2p} orbital. Both the B_{2p} orbital and the O_{2p} orbital contributed to the states below the Fermi level, and minimal hybridization can be found between the B_{2p} orbital and the O_{2p} orbital at around -0.5 eV. This suggests some bonding between 2-Thiouracil and BC_3, corresponding to physisorption, indicated by the adsorption energy of -0.247 eV shown in Table IV.

2. 2T-S/BC_3

The optimized structure of 2T-S/BC_3 is shown in Fig. 3(b). The binding distance is measured to be 3.49 Å, shown in Table IV.

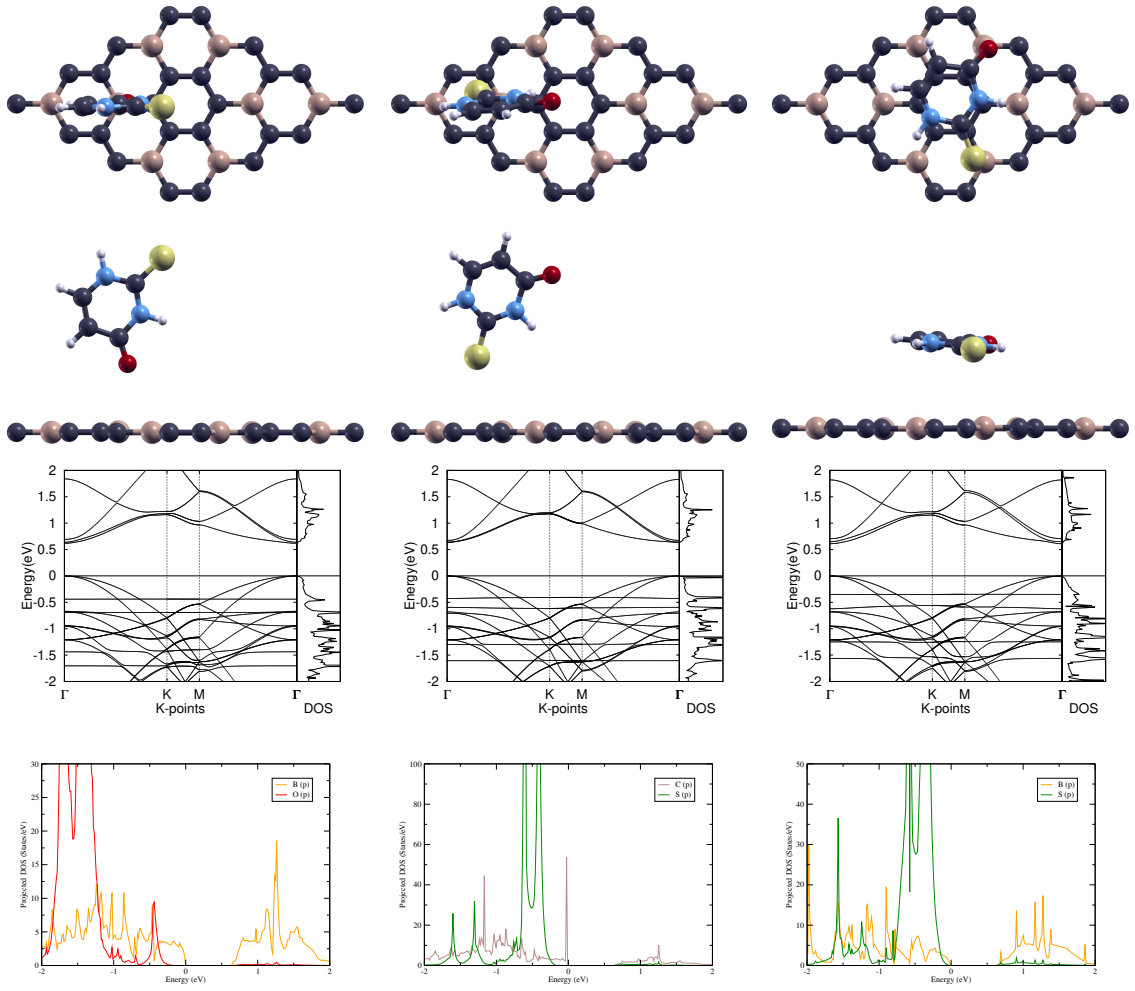

(a) (b) (c)

FIG. 3: Optimized configurations of 2-Thiouracil molecule on 3 different sites of pristine BC_3 monolayer, (a) 2T-O/BC_3, (b) 2T-S/BC_3, (c) 2T-h/BC_3. The first and second rows show the top and side views of the 3 configurations, respectively; carbon, boron, oxygen, nitrogen, hydrogen, and sulfur atoms are represented as purple, beige, red, blue, white, and yellow, respectively. The third row displays the calculated band structures and total DOS of each configuration, with the Fermi level set to 0 eV; the high symmetry k point circuit runs in the following order $\Gamma \rightarrow K \rightarrow M \rightarrow \Gamma$. The last row shows the projected DOS of two selected orbitals of each configuration; the B_{2p}, O_{2p}, C_{2p}, and S_{3p} orbitals are represented as yellow, red, brown, and green, respectively.

The direct band gap between the VBM and CBM at Γ point, shown in the band structure, is revealed to be 0.634 eV in Table IV. This band gap is smaller compared to the pristine BC_3 band gap of 0.648 eV in Table III, demonstrating changes in electronic structure due to adsorption. The total DOS shows the same band gap.

The projected DOS in Fig. 3(b) shows that the electron states around and above the Fermi level, 0 eV, were mainly contributed by the C_{2p} orbital. Moreover, both the C_{2p} orbital and the S_{3p} orbital contributed to the states below the Fermi level, and only very minimal hybridization can be found between the C_{2p} orbital and the S_{3p} orbital at around -0.7 eV, suggesting minimal interactions between the drug molecule and the monolayer and confirming physisorption and the calculated -0.288 eV adsorption energy in Table IV.

3. 2T-h/BC_3

The atomic structure of 2T-h/BC_3 after relaxation is shown in Fig. 3(c). The binding distance in Table IV, 3.51 Å, is similar to the other two configurations.

A direct band gap between the VBM and CBM at Γ point is displayed in the band structure. After 2-Thiouracil adsorption on BC_3, the band gap decreased from 0.648 eV to 0.611 eV, as shown in Table III and Table IV. This minimal change demonstrates evidence of interaction between 2-Thiouracil and pristine BC_3. The total DOS confirms the band gap of 0.611 eV.

In Fig. 3(c), the projected DOS shows that the electron states around and above the Fermi level, set to 0 eV, were contributed by mostly the B_{2p} orbital. Furthermore, both the B_{2p} orbital and the S_{3p} orbital contributed to the states below the Fermi level, and hybridization is observed at -1.6 eV, demonstrating evidence of bonding between BC_3 and 2-Thiouracil, which is also reflected by the largest adsorption energy of -0.559 eV out of all three positions shown in Table IV. However, this adsorption energy is still classified under physisorption.

Overall, although 2T-h/BC_3 has the largest adsorption energy, -0.559 eV, within the three complexes, weak physisorption is observed between the 2-Thiouracil molecule and the pristine BC_3 monolayer due to small adsorption energies and minimal hybridization shown in projected DOS.

TABLE IV: Adsorption energy E_{ad} (eV), lattice constant a (Å), band gap E_g (eV), and binding distance d (Å) of 2-Thiouracil on pristine BC_3. Phy represents physisorption, and dir represents direct band gap.

Complex	E_{ad} (eV)	a (Å)	E_g (eV)	d (Å)
2T-O/BC_3	-0.247 (phy)	10.350	0.619 (dir)	3.05
2T-S/BC_3	-0.288 (phy)	10.351	0.634 (dir)	3.49
2T-h/BC_3	-0.559 (phy)	10.351	0.611 (dir)	3.51

C. 2-Thiouracil adsorbed on Si-doped BC_3

2-Thiouracil was placed onto Si-doped-BC_3 in four positions, 2T-O/Si-BC_3, 2T-O_h/Si-BC_3, 2T-S/Si-BC_3, and 2T-S_h/Si-BC_3. O and S represent the atom on 2-Thiouracil placed closest to the Si dopant on the monolayer; configurations with h indicate a horizontal 2-Thiouracil molecule, as opposed to vertical. Top and side views of all four optimized structures are shown in the first two rows of Fig. 4. The computed band structures, total density of states (DOS), and projected DOS can be found below each atomic structure. Adsorption energy, lattice constant, band gap, and binding distance of each complex are shown in Table V.

1. 2T-O/Si-BC_3 The optimized atomic structure of 2T-O/Si-BC_3 is shown in Fig. 4(a). A chemical bond formed between the O atom and the Si atom, where a bump in the monolayer can be observed at Si. The binding distance is thus only 1.81 Å, as displayed in Table V.

The band structure showcases an indirect band gap of 0.294 eV between the VBM and CBM, shown in Table V. This band gap is larger than the 0.124 eV band gap of Si-BC_3 in Table III, showing changes in electronic structure after 2-Thiouracil adsorption. Moreover, a flat band can be observed at around 0.3 eV, and the total DOS also displays significant electron states at 0.3 eV, demonstrating the influence of the 2-Thiouracil molecule on the electronic structure.

The projected DOS in Fig. 4(a) reveals that both the Si_{3p} orbital and the O_{2p} orbital contributed to the states around, below, and above the Fermi level of 0 eV. While evidence of minimal overlapping of orbitals can be seen at all energy levels between -2 and 2 eV,

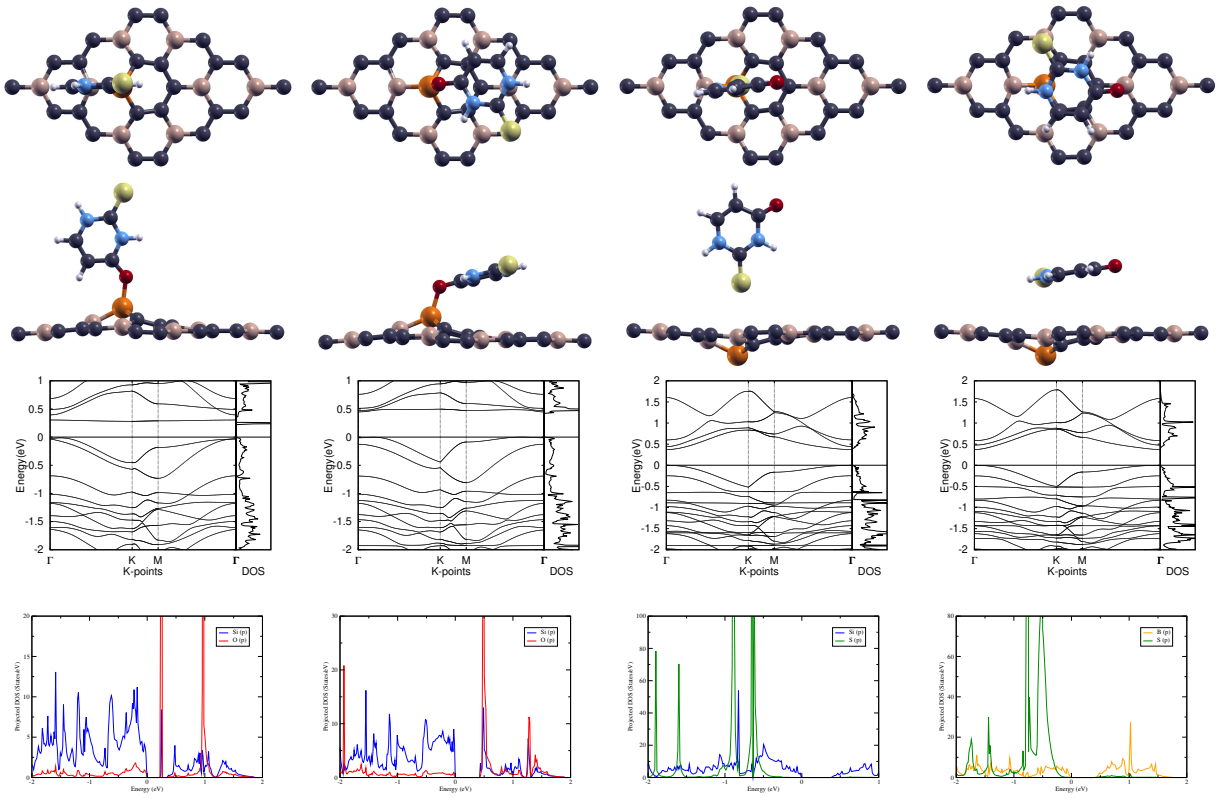

(a) (b) (c) (d)

FIG. 4: Optimized configurations of 2-Thiouracil molecule in 4 different positions on Si-doped BC_3 monolayer (a) 2T-O/Si-BC_3, (b) 2T-O_h/Si-BC_3, (c) 2T-S/Si-BC_3, (d) 2T-S_h/Si-BC_3. The first and second rows show the top and side views of the 4 optimized configurations, respectively; carbon, boron, silicon, oxygen, nitrogen, hydrogen, and sulfur atoms are represented as purple, beige, orange, red, blue, white, and yellow, respectively. The third row displays the calculated band structures and total DOS of each configuration, with the Fermi level set to 0 eV; the high symmetry k point circuit runs in the following order $\Gamma \rightarrow K \rightarrow M \rightarrow \Gamma$. The last row shows the projected DOS of two selected orbitals of each configuration; the Si_{3p}, O_{2p}, S_{3p}, and B_{2p} orbitals are represented as blue, red, green, and yellow, respectively.

strong hybridization between the Si_{3p} and O_{2p} orbitals can be observed at around 0.2 eV. This demonstrates evidence of strong adsorption, corresponding to chemisorption and the large adsorption energy of -1.854 eV in Table V.

2. 2T-O_h/Si-BC_3

The optimized atomic structure of 2T-O_h/Si-BC_3 is shown in Fig. 4(b). A bump in the monolayer can be observed at the Si dopant due to the formation of a chemical bond with O, resulting in a short binding distance of 1.83 Å in Table V.

A direct band gap of 0.460 eV, stated in Table V, is shown in the band structure between the VBM and CBM at Γ point. This band gap increased from the 0.124 eV band gap of the Si-BC_3 monolayer in Table V, showcasing evidence of adsorption. A flat band is displayed at around 0.5 eV, which is confirmed by the significant electron states at 0.5 eV shown in the total DOS, indicating molecule influence on the electronic structure.

The projected DOS in Fig. 4(b) shows the contribution of both the Si_{3p} and O_{2p} orbitals at, below, and above the Fermi level of 0 eV. Strong hybridization of the two orbitals can be observed above the Fermi level, between 0.5 eV and 1.5 eV. This evidence of bonding and chemisorption can be further proven by the large adsorption energy of -2.003 eV shown in Table V.

3. 2T-S/Si-BC_3 The optimized atomic structure of 2T-S/Si-BC_3 is shown in Fig. 4(c). No chemical bond was shown, and a dip in the monolayer at the Si atom can be observed due to the weak interaction between Si and S and potentially repulsion, leading to a large binding distance of 3.88 Å, shown in Table V. The repulsion may be due to the low reactivity and large atomic size of the S atom.

From the band structure, a direct band gap between the VBM and CBM at Γ point can be observed. After 2-Thiouracil adsorption, the band gap of Si-BC_3 increased from 0.124 eV to 0.372 eV, as shown in Tables III and V. This demonstrates some influence of 2-Thiouracil on the electronic structure of the complex.

The projected DOS in Fig. 4(c) shows that the S_{3p} orbital only contributed to electron states below the Fermi level, while the Si_{3p} orbital contributed at, below, and above the Fermi level of 0 eV. Moreover, there is very minimal hybridization between the two orbitals below the Fermi level between -1 eV and -0.5 eV, demonstrating weak adsorption and corresponding to the smaller adsorption energy of -0.964 eV displayed in Table V. Although small compared to other configurations, 2T-S/Si-BC_3 still demonstrates chemisorption.

4. 2T-S_h/Si-BC_3 The atomic structure of 2T-S_h/Si-BC_3 is shown in Fig. 4(d). In this configuration, the molecule is horizontal, and the S atom was originally placed closest

TABLE V: Adsorption energy E_{ad} (eV), lattice constant a (Å), band gap E_g (eV), and binding distance d (Å) of 2-Thiouracil on Si-BC_3. Che indicates chemisorption; ind and dir represent indirect and direct band gap, respectively.

Complex	E_{ad} (eV)	a (Å)	E_g (eV)	d (Å)
2T-O/Si-BC_3	-1.854 (che)	10.381	0.294 (ind)	1.81
2T-O_h/Si-BC_3	-2.003 (che)	10.290	0.460 (dir)	1.83
2T-S/Si-BC_3	-0.964 (che)	10.387	0.371 (dir)	3.88
2T-S_h/Si-BC_3	-1.213 (che)	10.402	0.374 (dir)	3.49

to the Si atom; the S atom moved away during relaxation onto a B atom, possibly due to repulsion between S and Si. Moreover, the monolayer also displayed a dip at the Si atom, potentially to relieve strain and reach a lower energy state. Therefore, as shown in Table V, the binding distance between the molecule and the monolayer is 3.49 Å.

A direct band gap between the VBM and CBM at Γ point is shown in the band structure. After 2-Thiouracil adsorption, the band gap of Si-BC_3 increased from 0.124 eV to 0.374 eV, as shown in Tables III and V, indicating some influence of the 2-Thiouracil molecule.

In Fig. 4(d), the projected DOS reveals that the S_{3p} orbital only contributed to electron states below the Fermi level, while the B_{2p} orbital contributed to states at, below, and above the Fermi level of 0 eV. Furthermore, S_{3p} and B_{2p} orbitals displayed some overlap between -2 eV and -1 eV, showcasing some adsorption. The adsorption energy of -1.213 eV in Table V further classifies this adsorption as chemisorption.

All molecule-monolayer complexes demonstrate chemisorption. Specifically, we observed that 2T-O/Si-BC_3 and 2T-O_h/Si-BC_3 resulted in the formation of chemical bonds, short binding distances, presence of flat bands, and the largest adsorption energies; projected DOS analysis also showcase strong hybridization between the 2-Thiouracil molecule and the Si-BC_3 monolayer. Within the two, 2T-O_h/Si-BC_3 demonstrated the largest adsorption energy of -2.003 eV. We also observed that in configurations where S was selected as the interacting atom with the monolayer, 2T-S/Si-BC_3 and 2T-S_h/Si-BC_3, the Si dopant dipped below the monolayer, resulting in long binding distances, small adsorption energies,

and minimal hybridization between the molecule and monolayer. Therefore, the O atom on 2-Thiouracil has stronger chemisorption to the Si dopant on Si-BC_3 than the S atom.

D. 2-Thiouracil adsorbed on Al-doped BC_3

2-Thiouracil was placed onto Al-doped-BC_3 in three positions, 2T-O/Al-BC_3, 2T-O_h/Al-BC_3, and 2T-S_h/Al-BC_3. O and S represent the atom on the molecule interacting with the Al dopant on the monolayer; h indicates horizontal molecule configuration, as opposed to vertical. Top and side views of their optimized atomic structures, band structures, total and projected DOS, are shown in Fig. 5. Adsorption energy, lattice constant, band gap, and binding distance of each complex are shown in Table VI.

1. 2T-O/Al-BC_3 and 2T-O_h/Al-BC_3

The optimized structure of 2T-O/Al-BC_3 is shown in Fig. 5(a). In 2T-O_h/Al-BC_3, shown in Fig. 5(b), the molecule was initially placed horizontally, but it became vertical after relaxation. Notably, the configuration is very similar to 2T-O/Al-BC_3, demonstrating that a vertical configuration of 2-Thiouracil is energy favorable. Both configurations display the formation of a chemical bond between O and Al, resulting in a bump in the monolayer at Al. For 2T-O/Al-BC_3 and 2T-O_h/Al-BC_3, the binding distances are 1.88 Å and 1.89 Å, as shown in Table VI, respectively.

In both band structures, direct band gaps between the VBM and CBM at Γ point are shown. Both the band gaps of 2T-O/Al-BC_3 and of 2T-O_h/Al-BC_3, 0.212 eV and 0.282 eV, are larger than the 0.166 eV band gap of Al-BC_3, as shown in Tables VI and III. This showcases changes in the electronic structures of the two configurations after 2-Thiouracil adsorption. Both band structures also showcase a partially flat band at around 0.5 eV, corresponding to significant electron states in the total DOS at the same energy level. This indicates influence of the molecule on the electronic structures of both complexes.

In the projected DOS for both 2T-O/Al-BC_3 in Fig. 5(a) and 2T-O_h/Al-BC_3 in Fig. 5(b), the Al_{3p} orbital contributed mostly to the states around the Fermi level, but both the Al_{3p} and O_{2p} orbitals contributed to states above and below the Fermi level. Moreover, hybridization can be observed between -2 and -1 eV as well as at around 1.6 eV between the Al_{3p} and O_{2p} orbital, demonstrating evidence of adsorption and bonding. This projected

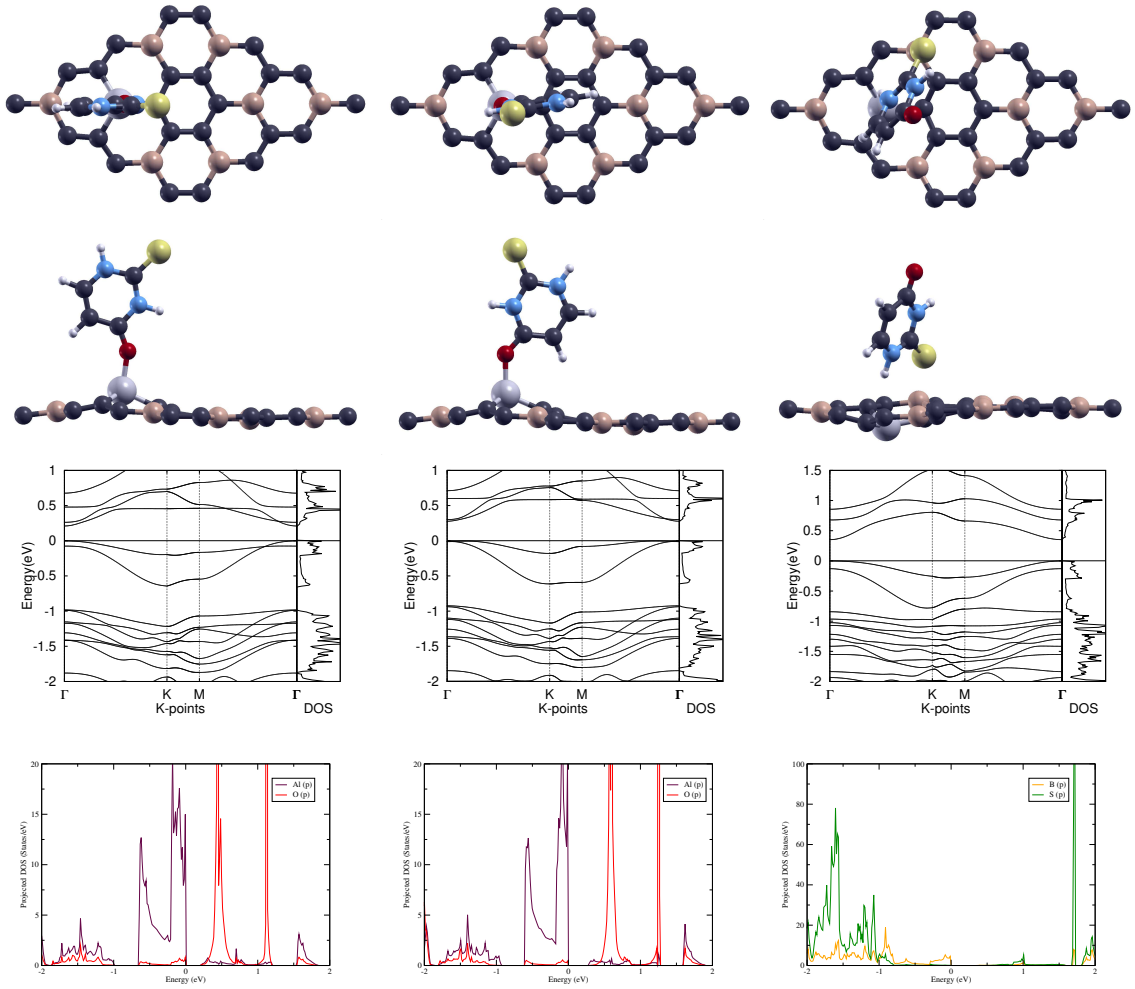

(a) (b) (c)

FIG. 5: Optimized configurations of 2-Thiouracil molecule in 3 different positions on Al-doped BC_3 monolayer (a) 2T-O/Al-BC_3, (b) 2T-O_h/Al-BC_3, (c) 2T-S_h/Al-BC_3. The first and second rows show the top and side views of the 3 optimized configurations, respectively; carbon, boron, aluminum, oxygen, nitrogen, hydrogen, and sulfur atoms are represented as purple, beige, grey, red, blue, white, and yellow, respectively. The third row displays the calculated band structures and total DOS of each configuration, with the Fermi level set to 0 eV; the high symmetry k point circuit runs in the following order $\Gamma \rightarrow$ K $\rightarrow$ M $\rightarrow \Gamma$. The last row shows the projected DOS of two selected orbitals of each configuration; the Al_{3p}, O_{2p}, S_{3p}, and B_{2p} orbitals are represented as maroon, red, green, and yellow, respectively.

DOS analysis corresponds to chemisorption and the large adsorption energies of -1.669 eV (2T-O/Al-BC_3) and -1.898 eV (2T-O_h/Al-BC_3).

2. 2T-S_h/Al-BC_3

The optimized structure of 2T-S_h/Al-BC_3 is shown in Fig. 5(c). After adsorption, the sulfur atom moved away from the Al atom onto a B atom, potentially due to the high-energy interaction and repulsion between S and Al. Furthermore, 2T-Al-BC_3-S in Fig. 5(c) showed no new bond and displayed a dip in the monolayer at the Al atom, demonstrating more evidence of repulsion for energy favorability. In Table VI, the binding distance between the 2-Thiouracil molecule and the Al-BC_3 monolayer is 2.13 Å, larger than the other two configurations. Notably, another structure where S was interacting with Al on the monolayer was originally computed, and resulted in the leaving of the 2-Thiouracil molecule from the monolayer, further displaying that the S atom would repel the Al dopant on the monolayer.

The direct band gap of 2T-S_h/Al-BC_3 is between the VBM and CBM at Γ point. After 2-Thiouracil adsorption, the band gap of Al-BC_3 increased from 0.166 eV to 0.353 eV, as shown in Tables III and VI, demonstrating a change in electronic structure after adsorption.

The projected DOS in Fig. 5(c) showed the contributions of both B_{2p} and S_{3p} orbitals to the electron states below and above the Fermi level, but at Fermi level, only B_{2p} contributed to the states. Moreover, some hybridization can be observed between -2 eV and -1 eV, demonstrating some interactions and corresponding to the adsorption energy of -1.210 eV in Table VI. Adsorption energy indicates chemisorption.

TABLE VI: Adsorption energy E_{ad} (eV), lattice constant a (Å), band gap E_g (eV), and binding distance d (Å) of 2-Thiouracil on Al-BC_3. Che indicates chemisorption, and dir represents direct band gap.

Complex	E_{ad} (eV)	a (Å)	E_g (eV)	d (Å)
2T-O/Al-BC_3	-1.669 (che)	10.509	0.212 (dir)	1.88
2T-O_h/Al-BC_3	-1.898 (che)	10.464	0.282 (dir)	1.89
2T-S_h/Al-BC_3	-1.210 (che)	10.464	0.353 (dir)	2.13

Overall, all configurations demonstrate chemisorption. 2T-O/Al-BC_3 and 2T-O_h/Al-

BC_3 resulted in very similar configurations, and both complexes displayed the formation of bonds, short binding distances, presence of flat bands, and large adsorption energies. Projected DOS analysis also showcases evidence of hybridization between orbitals of the molecule and the monolayer, demonstrating strong adsorption when O is placed on top of Al. We observed that when the S atom interacts with the Al atom on the monolayer in 2T-S_h/Al-BC_3, the Al atom dipped below the monolayer, resulting in small adsorption energies and long binding distances. The lack of hybridization also indicates weaker chemisorption. Therefore, similar to configurations of the Si-BC_3 monolayer, it was observed that the O atom on 2-Thiouracil has stronger chemisorption on Al than the S atom.

E. Charge Transfer

As 2T-O/Si-BC_3, 2T-O_h/Si-BC_3, 2T-O/Al-BC_3, and 2T-O_h/Al-BC_3 demonstrated successful adsorption, we wanted to conduct charge transfer calculations using Eq.3 to further investigate in electron density distribution caused by the adsorption of 2-Thiouracil.

The charge difference between the molecule and monolayers was calculated, and the isosurfaces for each configuration were plotted to visually represent the charge transfer results. The isosurfaces of 2T-O/Si-BC_3, 2T-O_h/Si-BC_3, 2T-O/Al-BC_3, and 2T-O_h/Al-BC_3 are displayed in Fig. 6(a), Fig. 6(b), Fig. 6(c), and Fig. 6(d), respectively. The 2T/Si-BC_3 configurations used the isovalue of 0.005 e/Bohr^3, and the 2T-Al-BC_3 charge transfer figures had an isovalue of 0.003 e/Bohr^3, indicating that there was more charge transfer between the molecule and Si-BC_3 than Al-BC_3. This further demonstrates that the Si-O bond is stronger than the Al-O bond.

In Fig. 6, all four configurations displayed considerable charge transfer. Red regions represent charge accumulation, and blue regions represent charge depletion. We observed that the 2-Thiouracil molecule, especially the O atom, always gains electron charge, while the doped BC_3 monolayers would lose charge at the dopant. This may be due to the high electronegativity and thus reactivity of O atoms compared to the dopants. Therefore, the considerable charge transfer between molecule and monolayer confirms the O atom's strong adsorption to the doped-BC_3 monolayers.

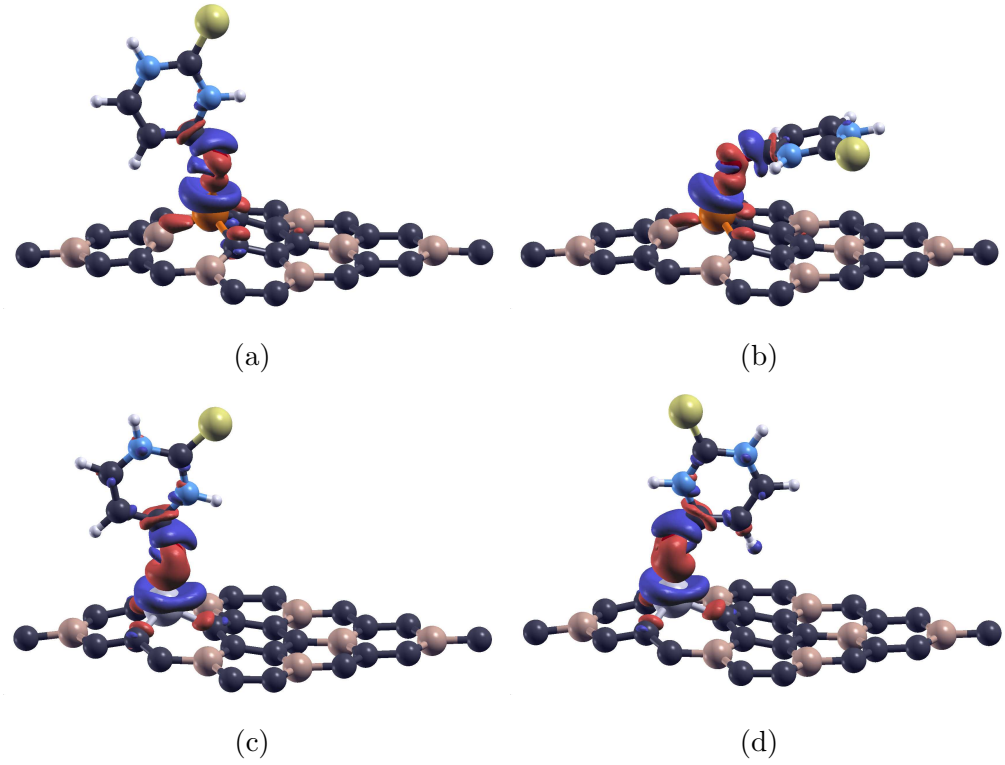

FIG. 6: Charge transfer of 2-Thiouracil molecule adsorbed on Si and Al doped BC_3 monolayers. (a) 2T-O/Si-BC_3, isovalue = 0.005 e/Bohr^3, (b) 2T-O_h/Si-BC_3, isovalue = 0.005 e/Bohr^3, (c) 2T-O/Al-BC_3, isovalue = 0.003 e/Bohr^3, (d) 2T-O_h/Al-BC_3, isovalue = 0.003 e/Bohr^3. Red regions indicate charge accumulation, and blue regions indicate charge depletion. Carbon, boron, silicon, aluminum, oxygen, nitrogen, hydrogen, and sulfur atoms are represented as purple, beige, orange, grey, red, blue, white, and yellow, respectively.

IV. CONCLUSION

Using first-principles calculations based on DFT, this study aimed to discover a novel drug delivery carrier for antithyroid drug 2-Thiouracil using pristine and doped graphene-like BC_3 monolayers. Our results indicate that the adsorption strength of 2-Thiouracil follows the trend: Si-doped BC_3 > Al-doped BC_3 > pristine BC_3. 2-Thiouracil on pristine BC_3 displays physisorption in all configurations, while molecule-monolayer complexes of both doped monolayers demonstrate chemisorption. When placing the 2-Thiouracil molecule on doped BC_3 monolayers, the O atom demonstrated stronger adsorption to the dopants than the S atom, primarily due to the O atom's high reactivity. Moreover, the Si-doped BC_3 demon-

strated more stable configurations and stronger adsorption of the 2-Thiouracil molecule than Al-doped BC_3. Among all configurations, 2T-O_h/Si-BC_3 showed the largest adsorption energy, making Si the most effective dopant and the horizontal O-binding configuration the most favorable for drug delivery. Although these results are based on first-principles calculations, they suggest that substitional doping BC_3 with Si could create a stable binding site for the O atom on 2-Thiouracil. Future work should evaluate biocompatibility, pH dependence, and stability in aqueous environments of the complex to assess its potential as a drug delivery platform for thyroid treatment.

[1] Davies, T. F.; Anderson, S.; Latif, R.; Nagayama, Y.; Barbesino, G.; Brito, M.; Kahaly, G. J. Graves' disease. *Nature Reviews Disease Primers* **2020**, *6(1)*, 52.

[2] Pokhrel, B.; Bhusal, K. *Graves Disease*; StatPearls Publishing, 2023; [Updated 2023 Jun 20]. Available from: `https://www.ncbi.nlm.nih.gov/books/NBK448195`.

[3] De Groot, L. J.; Bartalena, L.; Feingold, K. R. *Thyroid Storm*; MDText.com, Inc., 2022; [Updated 2025 Apr 15]. Available from: `https://www.ncbi.nlm.nih.gov/sites/books/NBK278927`.

[4] Chen, Y. K.; Lin, C. L.; Chang, Y. J.; Cheng, F. T.; Peng, C. L.; Sung, F. C.; Cheng, Y. H.; Kao, C. H. Cancer Risk in Patients with Graves' Disease: A Nationwide Cohort Study. *PubMed Central* **2013**, *23(7)*, 879–884.

[5] Brito, J. P.; Payne, S.; Ospina, N. S.; Rodriguez-Gutierrez, R.; Maraka, S.; Sangaralingham, L. R.; Iniguez-Ariza, N. M.; Montori, V. M.; Stan, M. N. Pattern of Use, Efficacy, and Safety of Treatment Options for Patients with Graves' Disease: A Nationwide Population-Based Study. *Thyroid* **2020**, *30(3)*, 357–364.

[6] Burch, H. B.; Cooper, D. S. Management of Graves Disease: A Review. *JAMA* **2015**, *314(23)*, 2544–2554.

[7] Liu, X.; Wong, C. K. H.; Chan, W. W. L.; Tang, E. H. M.; Woo, Y. C.; Lam, C. L. K.; Lang, B. H. H. Outcomes of Graves' Disease Patients Following Antithyroid Drugs, Radioactive Iodine, or Thyroidectomy as the First-line Treatment. *Annals of Surgery* **2021**, *273(6)*, 1197–1206.

[8] Awad, S. M.; Zohny, Y. M.; Ali, S. A.; Mahgoub, S.; Said, A. M. Design, Synthesis, Molecular Modeling, and Biological Evaluation of Novel Thiouracil Derivatives as Potential Antithyroid Agents. *Molecules* **2018**, *23(11)*, 2913.

[9] Senapati, S.; Mahanta, A. K.; Kumar, S.; Maiti, P. Controlled drug delivery vehicles for cancer treatment and their performance. *Signal Transduction and Targeted Therapy* **2018**, *3(1)*, 7.

[10] Byakodi, M.; Shrikrishna, N. S.; Sharma, R.; Bhansali, S.; Mishra, Y.; Kaushik, A.; Gandhi, S. Emerging 0D, 1D, 2D, and 3D nanostructures for efficient point-of-care biosensing. *Biosensors and Bioelectronics: X* **2022**, *12*, 100284.

[11] Paolino, D.; Cosco, D.; Gaspari, M.; Celano, M.; Wolfram, J.; Voce, P.; Puxeddu, E.; Filetti, S.;

Celia, C.; Ferrari, M.; Russo, D.; Fresta, M. Targeting the thyroid gland with thyroid-stimulating hormone (TSH)-nanoliposomes. *Biomaterials* **2014**, *35(25)*, 7101–7109.

[12] Zhang, Q. J.; Zhao, J. K.; Li, Y.; Wu, X. Y.; Ma, L. L.; Ding, Z. M. 5-Fluorouracil Trapping in a Porous Ba(II)-Organic Framework: Drig Delivery and Anti-Thyroid Cancer Activity Evaluation. *Russian Journal of Coordination Chemistry* **2024**, *503*, 237.

[13] Harismah, K.; Saeedi, N.; Rattanapan, N. Exploring Benefits of a Be-Doped Carbon Nanocone for the Drug Delivery of 2-Thiouracil: Computational Study. *Biointerface Research in Applied Chemistry* **2023**, *13(5)*, 481.

[14] Peng, L.; Mei, X.; He, J.; Xu, J.; Zhang, W.; Liang, R.; Wei, M.; Evans, D. G.; Duan, X. Monolayer Nanosheets with an Extremely High Drug Loading toward Controlled Delivery and Cancer Theranostics. *Advanced Materials* **2018**, *30(16)*, 1707389.

[15] Mahmud, K.; Yashir, T.; Zubair, A. First-principles calculations on monolayer WX2(X=S, Se) as an effective drug delivery carrier for anti-tuberculosis drugs. *Royal Society of Chemistry* **2024**, *6*, 2447–2458.

[16] Pari, A. A.; Yousefi, M.; Samadi, S.; Allahgholi Ghasri, M. R.; Torbati, M. B. Structural analysis of an iron-assisted carbon monolayer for delivery of 2-thiouracil. *Main Group Chemistry* **2021**, *20(4)*, 653–661.

[17] Ghuge, A. D.; Shirode, A. R.; Kadam, V. J. Graphene: A Comprehensive Review. *Current Drug Targets* **2017**, *18(6)*, 724–733.

[18] Geim, A. K. Graphene: Status and Prospects. *Science* **2009**, *324*, 1530–1534.

[19] Dastani, N.; Arab, A.; Raissi, H. DFT computational study towards investigating Cladribine anticancer drug absorption on the graphene and functionalized graphene. *Structural Chemistry* **2020**, *31*, 1691–1705.

[20] Khodadadi, Z.; Torkian, L. Studying metal-doped graphene nanosheet as a drug carrier for anticancer drug β-lapachone using Density Functional Theory (DFT). *Materials Research Express* **2019**, *6(6)*, 065058.

[21] Beniwal, S.; Hooper, J.; Miller, D. P.; Costa, P. S.; Chen, G.; Liu, S.; Dowben, P. A.; Sykes, E. C. H.; Zurek, E.; Enders, A. Graphene-like Boron-Carbon-Nitrogen Monolayers. *ACS Nano* **2017**, *11(3)*, 2486–2493.

[22] Luo, B.; Yao, Y.; Tian, E.; Li, L. Graphene-like monolayer monoxides and monochlorides. *PNAS*

2019, *116(35)*, 17213–17218.

[23] Zaman, A.; Shahriar, R.; Hossain, S. M. T.; Akhond, M. R.; Mumu, H. T.; Sharif, A. A graphene-like BeS monolayer as a promising gas sensor material with strain and electric field induced tunable response: a first-principles study. *RSC Advances* **2023**, *13*, 23558–23569.

[24] Mortazavi, B.; Shahrokhi, M.; Raeisi, M.; Zhuang, X.; Pereira, L. F. C.; Rabczuk, T. Outstanding strength, optical characteristics and thermal conductivity of graphene-like BC3 and BC6N semiconductors. *Carbon* **2019**, *149*, 733–742.

[25] Zhang, H.; Liao, Y.; Yang, G.; Zhou, X. Theoretical Studies on the Electronic and Optical Properties of Honeycomb BC3 monolayer: A Promising Candidate for Metal-free Photocatalysts. *ACS Omega* **2018**, *3(9)*, 10517–10525.

[26] Rahimi, R.; Solimannejad, M. BC3 graphene-like monolayer as a drug delivery system for nitrosourea anticancer drug: A first-principles perception. *Applied Surface Science* **2020**, *525*, 146577.

[27] Chen, W.; Li, S.; Wang, R.; Wu, X. Graphene-like BC3 and NC3 flakes as promisingh drug delivery systems. *Physica E: Low-dimensional Systems and Nanostructures* **2021**, *129*, 114633.

[28] Beheshtian, J.; Peyghan, A. A.; Noei, M. Sensing behavior of Al and Si doped BC3 graphenes to formaldehyde. *Sensors and Actuators B: Chemical* **2013**, *181*, 829–834.

[29] Moradi, M.; Noei, M.; Peyghan, A. A. DFT studies of Si- and Al-doping effects on the acetone sensing properties of BC3 graphene. *Molecular Physics* **2013**, *111(21)*, 3320–3326.

[30] Orio, M.; Pantazis, D. A.; Neese, F. Density functional theory. *Photosynthesis Research* **2009**, *102(2)*, 443–453.

[31] Gonze, X. et al. ABINIT: First-principles approach of materials and nanosystem properties. *Computer Physics Communications* **2009**, *180*, 2582–2615.

[32] Blochl, P. Projector augmented-wave method. *Physical Review B* **1994**, *50*, 17953–17979.

[33] Holzwarth, N. A. W.; Tackett, A. R.; Matthews, G. E. A Projector Augmented Wave (PAW) code for electronic structure calculations, Part I: atompaw for generating atom-centered functions. *Computer Physics Communications* **2001**, *135*, 329–347.

[34] Thakur, A.; Assad, H.; Kaya, S.; Kumar, A. In *Eco-Friendly Corrosion Inhibitors*; Guo, L., Verma, C., Zhang, D., Eds.; Elsevier, 2022; pp 283–310.

[35] Rani, K.; Prakash, J.; Vats, J. K.; Palafox, M. A.; Rastogi, V. K. Molecular structure and

vibrational spectra of 2-thiouracil: A comparison with uracil. *Asian Journal of Physics* **2017**, *26(11-12)*, 365–373.

[36] Tiekink, E. R. T. Crystal structure of 2-thiouracil. *Zeitschrift fur Kristallographie* **1989**, *187(1-4)*, 79–84.

[37] Bafekry, A.; Shayesteh, S. F.; Ghergherehchi, M.; Peeters, F. M. Tuning the band gap and introducing magnetism into monolayer BC3 by strain/defect engineering and adatom/molecule adsorption. *Journal of Applied Physics* **2019**, *126(14)*, 144304.

[38] Yanagisawa, H.; Tanaka, T.; Ishida, Y.; Rokuta, E.; Otani, S.; Oshima, C. Phonon dispersion curves of stable and metastable BC3 honeycomb epitaxial sheets and their chemical bonding: Experiment and theory. *Physical Review B* **2006**, *73*, 045412.

[39] Zhao, Z.; Yong, Y.; Gao, R.; Hu, S.; Zhou, Q.; Su, X.; Kuang, Y.; Li, X. Adsorption, sensing and optical properties of molecules on BC3 monolayer: First-principles calculations. *Materials Science and Engineering B* **2021**, *271*, 115266.

[40] Zhao, L.; Li, Y.; Zhou, G.; Lei, S.; Tan, J.; Lin, L.; Wang, J. First-principles calculations of stability of graphene-like BC3 monolayer and its high-performance potassium storage. *Chinese Chemical Letters* **2021**, *32(2)*, 900–905.

Declaration of Academic Integrity

The participating team declares that the paper submitted is comprised of original research and results obtained under the guidance of the instructor. To the team's best knowledge, the paper does not contain research results, published or not, from a person who is not a team member, except for the content listed in the references and the acknowledgment. If there is any misinformation, we are willing to take all the related responsibilities.

Names of team members
Shengtian Hong

Signatures of team members 

Name of the instructor **Xuan Luo**

Signature of the instructor 

Date August 21, 2025